A neurorobotic platform for locomotor prosthetic development in rats and mice

2016 J. Neural Eng. 13 026007

(http://iopscience.iop.org/1741-2552/13/2/026007)

OPEN ACCESS
IOP Publishing
Journal of Neural Engineering
J. Neural Eng. 13 (2016) 026007 (15pp)
doi:10.1088/1741-2560/13/2/026007

A neurorobotic platform for locomotor prosthetic development in rats and mice

Joachim von Zitzewitz[1,4], Leonie Asboth[1,4], Nicolas Fumeaux[1], Alexander Hasse[2], Laetitia Baud[1], Heike Vallery[3] and Grégoire Courtine[1]

[1] International Paraplegic Foundation Chair in Spinal Cord Repair, Center for Neuroprosthetics and Brain-Mind Institute, Swiss Federal Institute of Technology (EPFL), Lausanne, Switzerland
[2] Chair of Engineering Design, FAU University of Erlangen-Nuremberg, Erlangen, Germany
[3] TU Delft Robotics Institute, Delft University of Technology, Delft, The Netherlands

E-mail: gregoire.courtine@epfl.ch

Received 24 July 2015, revised 11 November 2015
Accepted for publication 21 December 2015
Published 9 February 2016

Abstract

Objectives. We aimed to develop a robotic interface capable of providing finely-tuned, multidirectional trunk assistance adjusted in real-time during unconstrained locomotion in rats and mice. *Approach.* We interfaced a large-scale robotic structure actuated in four degrees of freedom to exchangeable attachment modules exhibiting selective compliance along distinct directions. This combination allowed high-precision force and torque control in multiple directions over a large workspace. We next designed a neurorobotic platform wherein real-time kinematics and physiological signals directly adjust robotic actuation and prosthetic actions. We tested the performance of this platform in both rats and mice with spinal cord injury. *Main Results.* Kinematic analyses showed that the robotic interface did not impede locomotor movements of lightweight mice that walked freely along paths with changing directions and height profiles. Personalized trunk assistance instantly enabled coordinated locomotion in mice and rats with severe hindlimb motor deficits. Closed-loop control of robotic actuation based on ongoing movement features enabled real-time control of electromyographic activity in anti-gravity muscles during locomotion. *Significance.* This neurorobotic platform will support the study of the mechanisms underlying the therapeutic effects of locomotor prosthetics and rehabilitation using high-resolution genetic tools in rodent models.

S Online supplementary data available from stacks.iop.org/JNE/13/026007/mmedia

Keywords: robotics, spinal cord injury, neuroprosthetics, locomotion, balance

(Some figures may appear in colour only in the online journal)

1. Introduction

Neurorehabilitation is the only common medical practice to improve the recovery of locomotion after neurological disorders. Various gait robotic interfaces have been developed to facilitate and optimize locomotor training. These robotic interfaces can be divided into two broad categories. First, systems such as the BART device (Cai *et al* 2006, Hamlin *et al* 2015) or the Phantom (Hsieh and Giszter 2011) that guide hindlimb movements using rigid robotic arms (Fong *et al* 2005, Timoszyk *et al* 2005, Reinkensmeyer *et al* 2006) or soft pneumatic actuators (Song *et al* 2013). Second, bodyweight support systems that are designed to provide trunk assistance during treadmill-restricted stepping (Song and Giszter 2011, Oza and Giszter 2015) or overground locomotion in rats (Song and Hogan 2008, Dominici *et al* 2012, Hamlin *et al* 2015). The majority of these robotic

[4] These authors contributed equally to this work.

systems guide or assist lower limb movements while providing unidirectional support against gravity during treadmill-restricted conditions. This approach presents several limitations: (i) support is only provided in the vertical direction while multidirectional trunk motion is essential to produce efficient gait (Winter *et al* 1993); (ii) stepping on a treadmill does not require as much active participation as natural locomotion overground (van den Brand *et al* 2012); (iii) most of the developed systems restrict gait training to stepping on a treadmill, a condition that drastically differs from the rich repertoire of locomotor tasks underlying activities of daily living. To address these drawbacks, we previously designed a multidirectional trunk support system for rats (Dominici *et al* 2012). This robot assists balance and propulsion along four independent degrees of freedom while rats are progressing naturally within a large workspace. The robotic interface acts as a trunk postural neuroprosthesis that supports the rats against the direction of gravity, prevents falls, and facilitates forward motion.

Rehabilitation procedures aim to promote activity during training in order to mediate activity-dependent reorganization of the recruited neuronal networks (Timoszyk *et al* 2005, Cai *et al* 2006, Oza and Giszter 2014, Oza and Giszter 2015). Therefore, the degree of recovery correlates with the amount, intensity and quality of the performed motor activity during training (Dietz and Harkema 2004, Edgerton *et al* 2008). This understanding has triggered the development of neuroprosthetic interventions to manipulate neural activity directly within the brain and spinal cord, or indirectly through peripheral nerve or muscle stimulation (Barthelemy *et al* 2007, Mushahwar *et al* 2007, Courtine *et al* 2009, van den Brand *et al* 2012, Steuer *et al* 2013, Angeli *et al* 2014). For example, robot-assisted training facilitated by electrochemical neuromodulation of lumbar motor circuits promoted extensive reorganization of neuronal connections after a severe spinal cord injury (van den Brand *et al* 2012). This remodeling restored supraspinal control of locomotion in rats with an injury that led to permanent paralysis of both hindlimbs.

Closed-loop control algorithms based on the current neurobiomechanical state (Wenger *et al* 2014) or decoded motor intention (Song and Giszter 2011, Nishimura *et al* 2013) yield great potential to further improve robotic training and neuromodulation therapies. (Courtine and Bloch 2015). These developments rely on the design of next-generation technological platforms wherein robotic interfaces, neuromodulation therapies and multifaceted recording technologies are seamlessly integrated. However, current rehabilitation robots, neuroprosthetic systems and recording technologies have been conceived independently. Consequently, the implementation of closed-loop algorithms for real-time control of robotic and neuroprosthetic systems requires a complex system integration to synchronize and interface the various technologies necessary for each experiment. Here, we introduce a platform enabling the rapid and versatile integration of any analog or digital signal, and the ability to interface the processed information with any control system with a sampling frequency of up to 8 kHz.

Experimental robot-assisted rehabilitation procedures and neuroprosthetic interventions are primarily developed in rats (Timoszyk *et al* 2005, Udoekwere *et al* 2006, Hsieh and Giszter 2011). Compared to larger mammals, rats enable large-scale studies with statistically sound number of subjects, while presenting a size that is sufficient for chronically implanted neuroprostheses. The identification of the mechanisms underlying the therapeutic effects of experimental interventions plays a pivotal role in facilitating their translation into clinical applications for human patients (Duda *et al* 2014). The vast majority of experimental tools supporting the deconstruction of circuit-level and molecular mechanisms mediating therapeutic effects have been designed for mice. Previous studies have developed robotic training and pharmacological interventions in mice with complete SCI (Fong *et al* 2005, Cai *et al* 2006). However, the integration of robotic interfaces, neuroprosthetic technologies and neurophysiological recordings have not been yet achieved for this animal model. The precision required in order to provide adjustable trunk assistance to such a small and light animal while simultaneously allowing unconstrained displacements within a large workspace reaches the limit of current robotic concepts. To remedy these restrictions, we designed a robotic platform and experimental protocols that support equivalent rehabilitation procedures and closed-loop neuroprosthetic systems in mice and rats.

Our study is divided into three sections. First, we introduce a novel robotic interface that enables the gradual control of whole-body movements in freely behaving rats and mice, and describe the integration of this robot within a platform interfacing recording and stimulation technologies. Second, we validate the robotic interface in healthy and spinal cord injured animals, both rats and mice. Third, we provide an example of applications wherein a targeted level of muscle activity modulates robotic actuation in real-time during locomotion after spinal cord injury.

2. Methods

2.1. Robotic system providing adjustable multidirectional trunk support

We established a robotic platform allowing highly precise control of force and torque in order to provide mice and rats with adjustable trunk assistance along four independent degrees of freedom (DoFs; three translations, one rotation around the vertical axis) within a large workspace ($1 \times 0.8 \times 0.3$ m and 200°) (figure 1). For each degree of freedom, we aimed to achieve force control over the entire range of possible forces and torques, from zero-force to forces in the order of the animal's weight. This type of control scheme requires decoupling the inertia and friction of the massive robotic macrostructure from the animal over the entire workspace. To achieve this decoupling, we designed and fabricated a compliant interface applying the principles of series-elastic actuation (Pratt *et al* 1995), but extended to multiple directions (Dominici *et al* 2012).

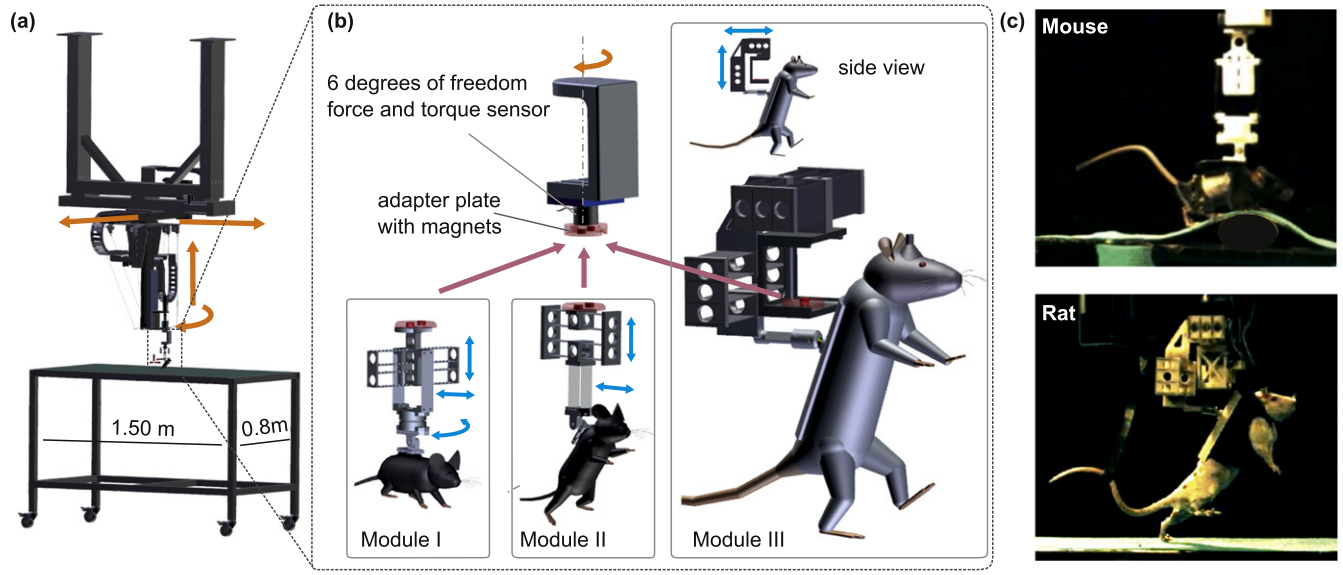

Figure 1. Robotic interface with exchangeable selective compliant modules. (a) The ceiling-mounted robotic macrostructure; the actuated degrees of freedom are highlighted with orange arrows. (b) Exchangeable, selective compliant modules are magnetically attached to a high-precision six DoF force/torque sensor mounted at the tool point of the macrostructure. The modules are exchanged based on the type of tested rodent or the performed locomotor task. The modules are shown for mice (Module I: three DoF; Module II: two DoF) and rats (Module III: two DoF). The blue arrows highlight the compliant DoFs of each module. (c) Picture of a mouse and a rat during quadrupedal and bipedal locomotion, respectively, performed while attached to the robotic interface.

We previously used this robotic principle to design a similar robotic interface for rats, which reached a 0.1 N precision in the control of forces. However, the bodyweight of mice is ten times smaller compared to rats. This drastic reduction requires increasing the precision of force control by a similar factor of magnitude. The compliant structure consisting of springs and linkages that we previously used, presents static friction that reached the same order of magnitude as a mouse's bodyweight. Consequently, the device cannot render forces at the required precision when interacting with mice.

To overcome these drawbacks, we utilized selective compliance modules (Hasse and Campanile 2009). In contrast to classical mechanisms combining rigid members and hinges, selective compliant modules exploit structural deformability to produce large displacements in selected directions while maintaining stiffness in the remaining DoFs. Selective compliant modules combine several key advantages, including the absence of wear, friction and backlash as well as reduced maintenance effort.

To achieve force control along various DoFs in either mouse or rat, we designed a robotic macrostructure covering the required workspace, with stiff actuation for all four DoFs, as well as selective compliant modules that can be attached to the macrostructure. Each of these compliant modules is dedicated to a specific application, in either rats or mice. The corresponding soft DoFs of a specific module consists of a serial concatenation of single-DoF elements (figure 2).

Parallel hinges cover the translational DoFs, while cross-spring pivots enable the rotational DoF (figure 2(a)). The ability to modulate trunk assistance around the rotatory DoF is an important component to train balance after spinal cord injury and curve walking (Dominici *et al* 2012, Waeber *et al* 2015). We defined the required compliance of the soft DoFs through scaling the results obtained in rats (Dominici *et al* 2012) to the mouse's bodyweight (table 1).

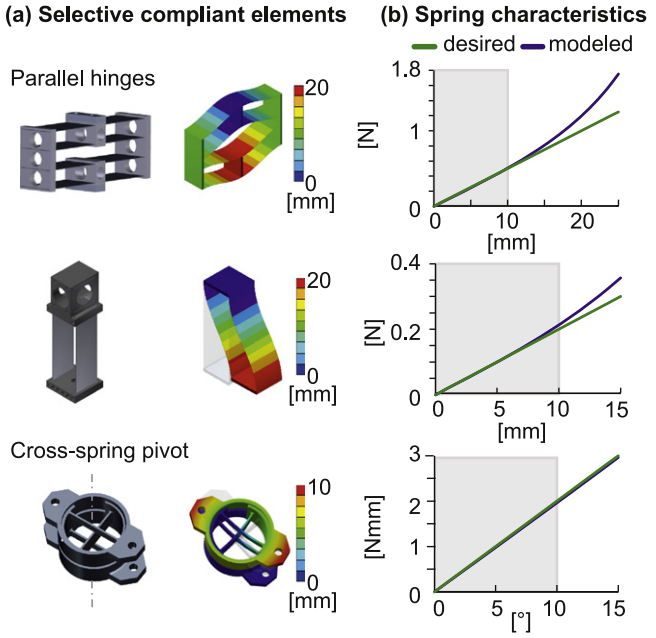

Figure 2. Characteristics of the constitutive elements of selective compliant modules. (a) 3D computer assisted design (CAD) models of the various modules exhibiting selective compliance in single translatory and rotational DoFs, together with the finite-element analysis of these modules. (b) Plots reporting the desired and modeled spring characteristics of each module. The shaded area highlights the range over which robotic actuation is needed based on species- and task-specific features.

Table 1. Stiffness of single elements of the selective compliant modules.

	Module I	Module II	Module III
Vertical	43 N m^{-1}	43 N m^{-1}	400 N m^{-1}
Horizontal	19 N m^{-1}	19 N m^{-1}	120 N m^{-1}
Rotational	—	0.20 Nmm/°	—

The single-DoF elements were designed to ensure the desired compliance while preventing occurrence of mechanical damage to the structure within the range of motion. The corresponding method is detailed in appendix A. The stiffness of the different elements in their respective DoF, elaborated by finite element calculations, is shown in figure 2(b). The stiffness is linear within the working range of the module (shaded area, figure 2(b)). To demonstrate the selective compliant behavior of Module I, which contains all three different elements (figure 1(b)), we also calculated the resistance against forces and torques in the remaining three stiff DoFs using finite element methods. The stiffness of the soft and stiff DoFs differed by several orders of magnitude. The single elements, which were manufactured as hybrid structures using thermoplastic material and spring metal, were assembled to obtain a selective compliant module with the required compliant DoFs.

The different selective compliant modules are attached to a high-precision 6D force/torque senor (FTD-Nano-17-Ti, ATI, NC, USA) using a pair of magnets that allows the fast exchange of the three modules (figure 1(b)). To cope with the ten-fold difference in weight and force between mice and rats, a double-calibration of the sensor was performed, providing two different measurement ranges and resolutions for mice (resolution of 0.003 N for forces, 0.014 N m for torque) and rats (resolution of 0.006 N, 0.027 N m). The control logic of the robot automatically switches between voltage supplies correlated to the two sensor calibrations depending on the weight of the module attached.

The forces/torques measured by the force sensor served as an input to the force control loop. For this purpose, we implemented the control strategy previously described for the control of the rat robotic interface (Dominici *et al* 2012). This control strategy limited the bandwidth of the robotic device (Eppinger and Seering 1987). However, the low stiffness of the selective compliant modules compensated for this limitation, minimizing the force modulation resulting from high-frequency movements. The selective compliant module directly determines the bandwidth, and thus the characteristics of the robot. Consequently, we limited the characterization of the robot to the vertical DOF of the mouse module (Module I in figure 1), which demanded the highest degree of precision to enable well-balanced gait execution. The measured bandwidth remained within the order of 3 Hz (see appendix B). In order to illustrate the adequate interplay of the control scheme and the elastic properties of the selective compliant modules, we conducted experiments in healthy mice across challenging conditions requiring high-precision force control (section 2.5).

In addition to force control, each DoF of the robot can also be moved in position control mode.

2.2. Real-time robotic and neuroprosthetic platform

We designed a technological platform that integrates (i) a physiological recording unit monitoring and integrating kinematics and analog signals, (ii) the robotic system described above, and (iii) a control processing unit adjusting control policies in real-time (figure 3). All three units are interconnected via an Ethernet network.

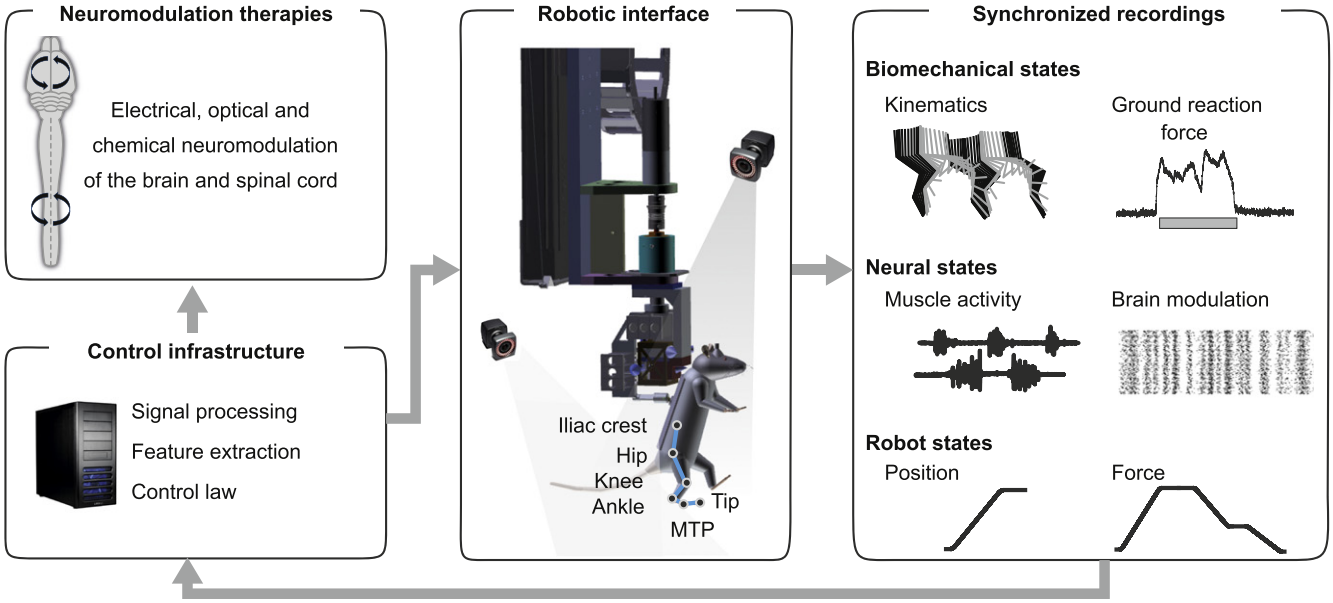

Figure 3. Design and structure of the neurorobotic platform. The robotic interface is integrated within a real-time monitoring and control platform. Biomechanical, neural, and robot states are recorded synchronously and available in real-time (EtherCAT, 2 kHZ) to the control infrastructure that adjusts neuromodulation therapies or robotic actuation in closed-loop. MTP, metatarsophalange.

The recording unit includes a marker-based, infrared motion capture system (Bonita, Vicon, Oxford, UK) for monitoring whole limb movements (sampled at 200 Hz), and the Nexus software to integrate and synchronize analog signals sampled at 2 kHz. The analog inputs are used to record electromyographic activity as well as ground reaction forces from a small force plate (figure 3).

All sensor signals of the robotic system are fed into a real-time Ethernet-based fieldbus system (EtherCAT) via Ethercat terminals (Beckhoff, Verl, Germany) connected to the common Ethernet network. These terminals allow synchronized recordings of the majority of common analog and digital signals. Dedicated oversampling terminals are used to acquire the signals from the force sensor of the robotic sensor (ten values per sampling step), in order to improve signal quality and avoid aliasing effects. All the states of the robot derived from the inputs of the sensor, and the characteristics of ongoing control policies are constantly available on the EtherCAT bus.

Signals on the EtherCat bus are processed in the control unit with a sampling frequency of 2 kHz. The control unit either controls force/torque or position of each robot axis independently.

To interconnect the physiological recording unit and the control processing unit, a fieldbus-independent automation device specification (ADS) interface is used as an intermediate layer. Signals from the recording unit are read in by the control unit through the C++−based DataStream SDK from Vicon (http://vicon.com/products/software/datastream-sdk) and transmitted to the real-time controller via the ADS interface. Signals on the EtherCat bus are sent via the ADS interface to the recording unit and added to the string of recorded signals using the C++−based Digital Device SDK from Vicon. The total round-trip delay of a signal sent out by the physiological recording unit, processed by the control processing unit, and returned to the physiological recording unit remains below 20 ms. This latency originates from the delays in the motion capture system. All other measures on the EtherCat bus are transferred within sub-millisecond precision. Therefore, neuroprosthetic systems integrating muscle activity or brain modulation operate well below this latency. This closed-loop control structure allows adaptation of the desired force or speed for each robotic DoF independently based on the current state of the animal, as measured by the physiological recording unit.

2.3. Animal models and surgical procedures

All surgical procedures conducted in rodents were performed in accordance with Swiss federal legislation and under the guidelines established at EPFL and approved by local Swiss Veterinary Offices. Experiments on rats were performed on female Lewis rats, with an initial weight 180–200 g. For mice, C57Bl/6JRJ female mouse strains with an initial weight of 15–35 g were used. Spinal cord contusion was induced in both rats and mice using an IH-400 Impactor with adjusted force levels relative to the species (250 kDynes for rats and 80 kDynes for mice). Laminectomy was performed at T8 vertebrae (T9 spinal segment). Within the same surgery, some of the animals were implanted with electrodes over the dorsal aspect of spinal segments L2 and S1. Electrodes were created by removing a small part (1 mm notch) of insulation from Teflon-coated stainless steel wires (AS632, Cooner Wire) as previously described in rats (Wenger *et al* 2014). In mice, we used small diameter PFA coated stainless steel wires (A-M systems, WA, US). The wires were attached to a connector (Omnetics, MN, US) that was fixed onto the skull with dental cement. Some of the animals were implanted with a pair of electrodes into extensor muscles (vastus lateralis in mice or Gastrocnemius medialis in rats) and flexor muscles (tibialis anterior) to record electromyographic activity (Takeoka *et al* 2014, Wenger *et al* 2014). To enable locomotion after injury, the animals were tested under electrical and pharmacological neuromodulation of the spinal cord. A serotonergic replacement therapy combining the 5HT2A agonist quipazine and the 5HT1A/7 agonist 8-OHDPAT was administered intraperitoneally (Musienko *et al* 2011). Electrical stimulation was delivered through each epidural spinal cord electrode using A-M system stimulators (A-M systems, WA, US). We delivered charge-balanced pulses at 40 Hz with a 0.2 ms duration, and intensities ranging from 100 to 200 μA (Courtine *et al* 2009).

2.4. Animal attachment to the robotic system

Previous studies have developed surgically implanted pelvis orthoses to attach the experimental subjects to robotic interfaces (Udoekwere *et al* 2006, Song and Hogan 2008, Hsieh and Giszter 2011, Song and Giszter 2011, Udoekwere *et al* 2014). This method avoids altered sensory feedback from slings, cuffs, and jackets. In addition, this rigid attachment allows an efficient high-bandwidth mechanical coupling to a robot since this interface has no impact on force transmission. Here, we opted for a non-implantable solution for two main reasons. First, our aim was to support evaluation and training of both bipedal and quadrupedal locomotion in the same subjects. However, the required attachment points for bipedal and quadrupedal gait support are completely different. Evaluation and training of animals in both postures, which is essential for our experiments, would have required the implantation of two types of orthoses in each animal. Therefore, we focused on a less-invasive though easy and translational method to attach the animals to the robot. Second, additional elasticity and damping have a positive influence on the force control performance in our setup. The increased compliance at the end-effector improves stability (Pratt and Williamson 1995) and allows for higher control gains compared to a stiff coupling (Colgate and Hogan 1989), while decreasing the change in interaction force resulting from high-frequency movements (Vallery *et al* 2008).

In order to attach healthy mice for quadrupedal tasks to the robot, a layer of permeable tape was wrapped around the trunk of the mouse. A Velcro piece was positioned on the tape, enabling attaching the mouse to the robot. After testing, alcohol was applied onto the permeable tape to dissolve the

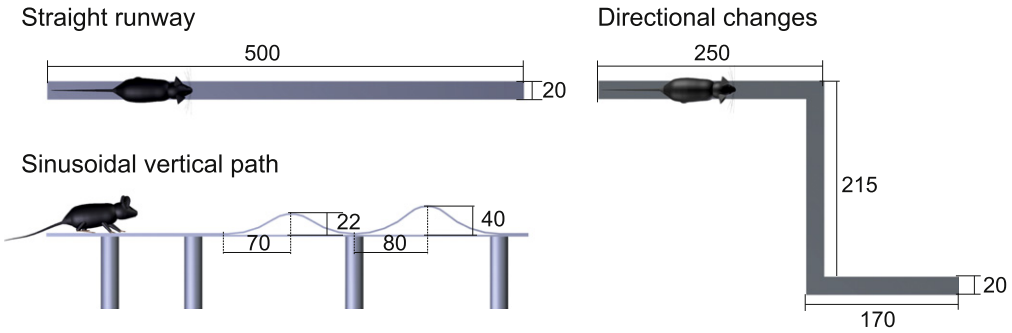

Figure 4. Tested locomotor tasks. Specific runways were fabricated to evaluate the performance of the robotic interface. Units, millimeters.

glue and withdraw the tape from the mouse. For bipedal locomotion, mice wore a custom-made upper-body jacket with a Velcro that allowed attaching them to the robot. The jacket was a down-scaled version of the jacket developed for rats and described in detail previously (Dominici *et al* 2012).

2.5. Behavioral experiments

We performed experiments in healthy and contused mice. Healthy mice were first trained during one week to walk along a straight runway, a runway requiring sharp directional changes and a runway with a path following a vertical sinusoid (figure 4).

Injured mice were tested in both bipedal and quadrupedal postures. Injured rats were only tested in a bipedal posture. We also tested the subjects during guided locomotor execution. We used two control modes. In the first condition, the robotic interface was set to position-control mode in which the subject was moved in the forward walking direction at a pre-defined velocity, set to 11 cm s^{-1} for mice and 13 cm s^{-1} for rats. In parallel, the subject received a force-controlled trunk assistance against the direction of gravity, which was adjusted for each subject in order to obtain optimal performance. In the second condition, the robot was configured in a force-control mode in the forward walking direction. The evaluated horizontal forces ranged between 0% and 20% of the subject's body-weight. In the zero-force mode, the subject had to deliver a supraspinal drive to spinal circuits in order to move forward. The addition of horizontal forces facilitates the forward displacement, progressively replacing the supraspinal drive with an increasing amount of forward force. The subjects were tested in a spontaneous condition, under chemical neuromodulation, or under electrochemical neuromodulation.

2.6. Kinematic, kinetic and muscle activity recordings

All procedures used have been detailed previously (Dominici *et al* 2012, Takeoka *et al* 2014). Bilateral hindlimb kinematics were captured by the high-speed motion capture system Vicon, as described above. Reflective markers (1 mm) were attached bilaterally at the iliac crest, the greater trochanter (hip joint), the lateral condyle (knee joint), the lateral malleolus (ankle), the distal end of the fifth metatarsophalangeal (MTP) joint and, for rats, a fifth marker was placed at the tip of the fourth toe. The body was modeled as an interconnected chain of rigid segments, and joint angles were generated accordingly. Ground reaction forces were recorded using a biomechanical force plate (2 kHz; HE6X6, AMTI, USA) located in the middle of the runway. EMG signals (2 kHz) were amplified, filtered (10–1000 Hz bandpass), stored and analyzed offline to compute the amplitude, duration and timing of individual bursts. For both the left and right hindlimbs, 15 successive step cycles were typically extracted over several trials on the runway for each subject under each experimental condition. A 20 s interval was used when no or very minimal hindlimb movements were observed.

2.7. Analysis of kinematics, kinetics, and muscle activity

A large number of parameters quantifying kinematics, kinetics, and muscle activity features were computed for each hindlimb and gait according to methods described in detail previously (Dominici *et al* 2012, Takeoka *et al* 2014). To evaluate differences between experimental conditions and groups, as well as the most relevant parameters to explain these differences, we implemented a multi-step statistical procedure based on principal component (PC) analysis (Takeoka *et al* 2014). PC analyses were applied on data from all individual gait cycles for all the subjects together. Data were analyzed using the correlation method, which adjusts the mean of the data to 0 and the SD to 1. This method of normalization allows the comparison of variables with disparate values (large vs. small values) as well as different variances. We quantified differences between experimental conditions as the distance between gait cycles in the 3D space created by PC1-3 (van den Brand *et al* 2012).

2.8. Anatomical evaluation of spinal cord injury

All the subjects were deeply anesthetized by an intraperitoneal injection of Pentobarbital-Na and transcardially perfused with Ringer's solution containing 100 000 IU l^{-1} heparin (Liquemin, Roche, Switzerland) and 0.25% $NaNO_2$ followed by cold 4% phosphate buffered paraformaldehyde, pH 7.4 containing 5% sucrose. The spinal cord was removed and postfixed in the same fixative before they were transferred to 30% sucrose in phosphate buffer (PB) for cryoprotection. The tissue was embedded in Tissue Tek O.C.T (Sakura Finetek Europe B.V., The Netherlands), frozen at −40 °C, and cut to a thickness of 40 μm. Sections were pretreated with 0.03% H2O2. Mounted

sections were washed three times in 0.1 M PBS and blocked in 10% normal goat serum containing 0.3% Triton. Sections were then incubated in rabbit anti-GFAP antibody (1:1000, Dako, USA) diluted in the blocking solution overnight at 4 °C. Sections were again washed three times in 0.1 M PBS and incubated with a secondary antibody (Alexa fluor® 488 Molecular Probes, Life Technologies, USA) in blocking solution. Slides were finally washed, air-dried and coverslipped with Mowiol. The extent and location of spinal cord damage was evaluated in each experimental subject. The entire extent of the lesion cavity was reconstructed in three dimensions using Neurolucida (MBF Bioscience, USA).

2.9. Statistical analysis

All data are reported as mean values ±s.e.m.. In trials using single subjects, statistics were performed on kinematic parameters calculated across a large series of steps. We used Student's t-test between normally distributed data (Kolmogorov-Smirnov test) from the different experimental conditions. When using a small cohort of subjects, we carried out Mann-Whitney tests between the various experimental conditions. In experiments performed on cohorts of subjects with more than two testing conditions, a Kruskal–Wallis test was applied over the means of the group. Post hoc comparisons using Bonferroni's correction were applied if the null hypothesis of the Kruskal–Wallis test was rejected.

3. Results

3.1. Evaluation of the transparency of the robotic interface

We first evaluated the zero-impedance control mode of the robotic interface in healthy mice with a body weight below 25 g (figure 5(a)). Our objective was to assess whether the robotic interface was capable of following the mice along simple and complex locomotor paths without impeding gait pattern features. For these experiments, the required degrees of freedom of the robotic interface were set to zero-impedance control mode, i.e. the chosen axes behaved transparently. We compared kinematic parameters in healthy mice walking quadrupedally along a straight runway (figure 4). The mice walked freely or attached to the robotic interface. Detailed analyses revealed no significant changes in gait patterns between both conditions, even for sensitive parameters such as stride length, maximum velocity of foot trajectory and 3D displacements of the pelvis segments ($p > 0.05$, figure 5(b)).

These results demonstrate that the robotic interface does not interfere with the natural walking movements of mice on a straight runway, which is the most common experimental scenario. We next sought to challenge the robotic interface with more complex locomotor executions requiring changes in directions, both in the mediolateral and vertical directions. For this purpose, we trained the mouse to walk along runways with abrupt changes in directions or vertical bumps (figure 4). Even in these extreme conditions, the robotic interface did not impede the natural flow of walking movements (figures 5(c) and (d) and movie 1). The mouse occasionally paused during execution and remained still or groomed before resuming the locomotor execution. The robotic interface smoothly followed these natural behaviors (movie 1).

3.2. Position-control mode imposes locomotion in injured mice and rats

We then exploit the position-control mode of the robotic interface to test the effect of chemical neuromodulation during involuntary locomotion. For these evaluations, the axis related to the forward walking direction moved the subjects at a constant velocity (11 cm s^{-1} for mice, 13 cm s^{-1} for rats) while providing adjustable trunk assistance in the vertical direction. We tested both mice and rats that had received a spinal cord contusion three weeks prior to testing. The lesion led to complete hindlimb paralysis. Spontaneously, both mice and rats dragged both hindlimbs along the runway (figure 6), as observed when positioning paralyzed subjects over a moving treadmill belt (not shown).

To enable functional states of spinal circuits, we delivered a serotoninergic replacement therapy consisting of agonists to 5HT1A and 5HT2A receptors (see methods). Under these conditions, both mice and rats transited from tonic activity in extensor muscles during stance to an alternative recruitment of flexor and extensor muscles associated with coordinated planter stepping movements as soon as the robotic interface moved their body forward (movie 2). These experiments demonstrate that the robotic interface is capable of controlling the position of the subjects while providing adjustable vertical trunk assistance, enabling coordinated locomotion in injured mice and rats. The versatility of the platform allowed the rapid and straightforward exchange of the attachment module in order to switch between experiments in mice (<25 g) and rats (>200 g).

3.3. Horizontal support facilitates locomotion in injured mice

We evaluated the impact of horizontal support forces in the force-control mode on the facilitation of locomotor execution in mice with spinal cord contusion (figure 7(a)). The paralyzed mice received the serotoninergic replacement therapy to enable locomotor states (figure 7(b)). The amount of vertical trunk assistance was adjusted to maximize loading and stepping quality based on visual observations. Without horizontal trunk assistance, none of the mice were able to initiate locomotion in the forward direction, and instead stepped in place (figure 7(c)). We then tested the effects of horizontal assistance ranging from 5% to 20% of their body weight. The amount of horizontal assistance modified the postural orientation of the body, promoting a gradual forward tilt of the trunk, as emphasized with the blue dotted line in figure 7(c). The gradual increase in the degree of horizontal assistance progressively improved the robustness of locomotor movements, allowing the mice to move forward with significantly improved gait patterns. These improvements were captured

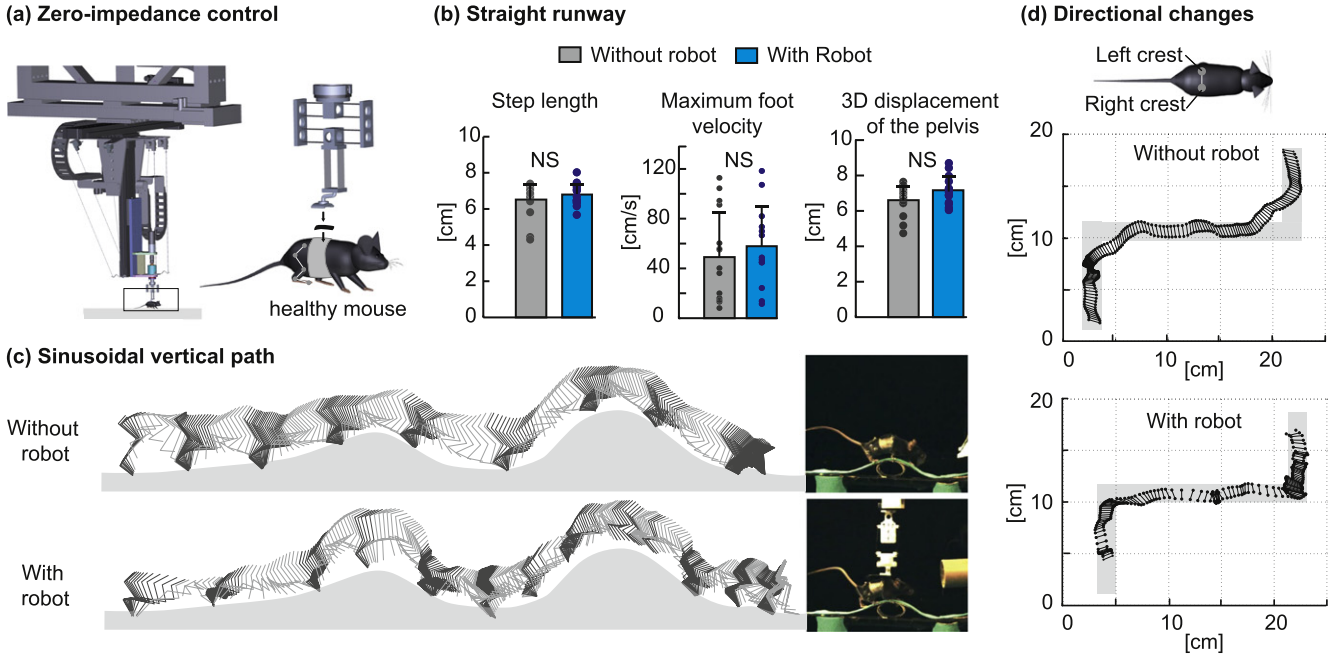

Figure 5. Transparency of the robotic interface in healthy mice. (a) The robotic interface was set to zero-force control mode. The healthy mouse was attached to the selective compliant module and reflective markers were placed on anatomical landmarks to record kinematics. (b) Bar graphs reporting the average values of relevant gait parameters while progressing along the straight runway with and without the attachment to the robotic interface. Single dots represent individual measurements for each gait cycle. (c) Representative stick diagram decomposition of hindlimb movements while progressing along a path following a vertical sinusoid. (d) Representative stick diagram decomposition of pelvis movements from a top view while progressing along a runway requiring abrupt changes in locomotor direction. Error bars, s.e.m.

by a PC analysis applied on 98 gait parameters. For example, the increase in horizontal assistance enabled the mice to produce increasingly larger stride lengths and velocities of foot trajectories during swing (figure 7(c)).

3.4. Force-control mode reveals synergy between electrical and chemical neuromodulation in injured mice and rats

We exploited the force-control mode of the robotic interface to test whether the combination of chemical and electrical neuromodulation of the lumbar spinal cord was capable of promoting superior facilitation of locomotion after spinal cord contusion, both in mice and rats. The subjects were implanted with two electrodes on the dorsal aspects of the lumbar and sacral spinal cord. The vertical and horizontal axes of the robotic interface were configured prior to recordings in order to provide optimal assistance to the mice and rats (figure 8(a)). The subjects were then recorded with the serotoninergic replacement therapy (chemical neuromodulation only) or with the serotoninergic replacement therapy and continuous electrical spinal cord stimulation (electrochemical neuromodulation; 40 Hz, 0.2 ms, 100–200 μA). Compared to chemical neuromodulation only, the combination of both chemical and electrical neuromodulation significantly improved gait patterns (figure 8(a)). For example, both mice and rats displayed reduced stance duration (figure 8(b)) and increased consistency of stepping movement (figure 8(c)).

3.5. Robotic assistance instantly improves quadrupedal locomotion in injured mice

We next evaluated whether the robotic interface was capable of providing appropriate vertical and mediolateral trunk assistance in order to facilitate quadrupedal locomotion of injured mice. The robotic interface was configured to provide adjustable assistance in the vertical direction (force-control) and prevent mediolateral falls, while behaving transparently in the forward walking direction (zero-impedance control). The mice were tested at three weeks after moderate spinal cord injury. In the absence of robotic assistance, the mice displayed highly variable stepping movements. The mice rarely exhibited plantar stepping, and instead showed extensive dragging of both hindlimbs during the swing of gait (figure 9(a) and movie 3). The vertical and mediolateral trunk assistance instantly improved locomotion. The mice produced reproducible plantar stepping movements with reduced dragging ($P < 0.05$; figure 9(c)), and significantly increased movement range of the hindlimb ($P < 0.001$ and $P < 0.01$; figure 9(c)), and decreased variability of hip, knee and ankle joint angles (figure 9(b)).

3.6. Closed-loop control of muscle activity via robotic vertical assistance

In a final experiment, we exploited the versatility of the developed neurorobotics platform. We aimed to develop a closed-loop control policy which automatically adapted robotic assistance based on neural states of the animal. For

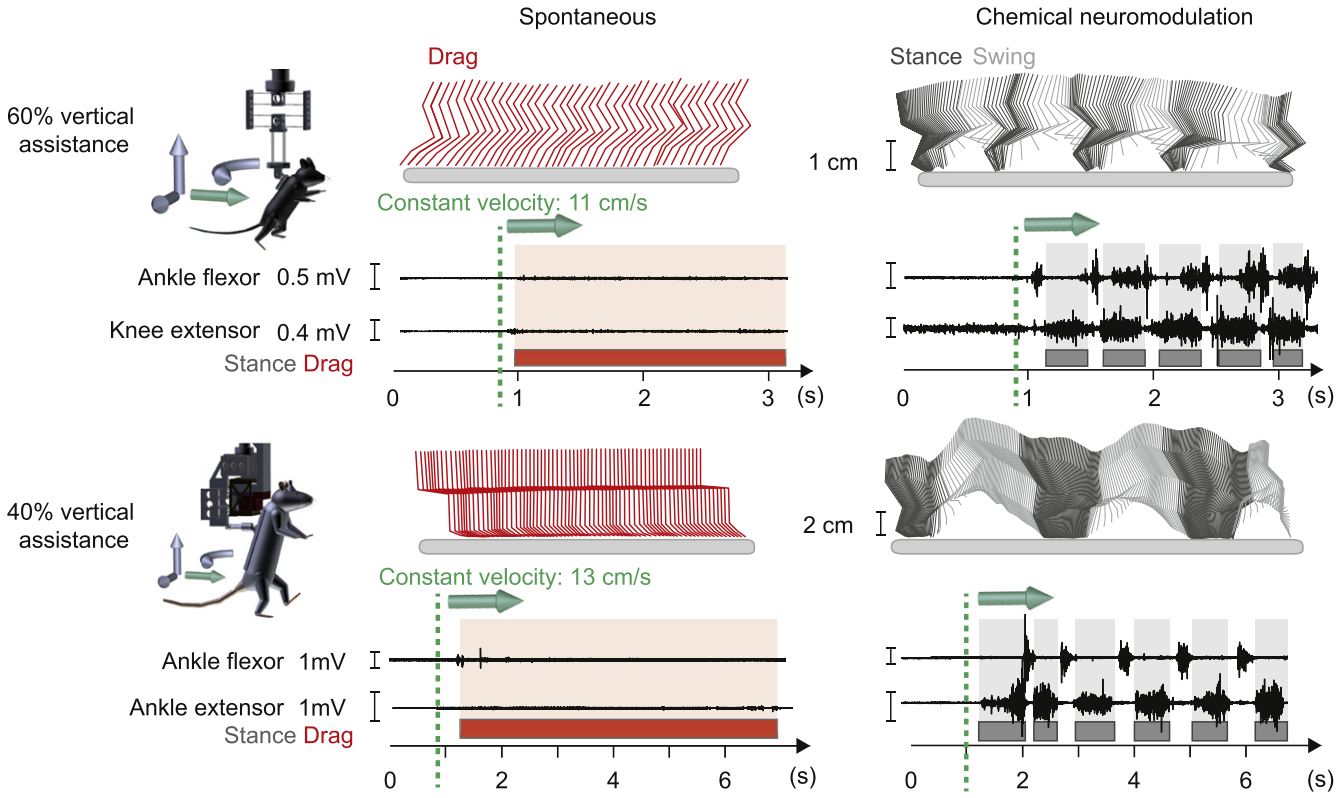

Figure 6. Robotic trunk assistance and chemical neuromodulation instantly enable locomotion in mice and rats with spinal cord injury. Rat and mouse received a severe contusion of thoracic spinal cord that led to complete hindlimb paralysis. The robotic interface provided personalized trunk assistance against the direction of gravity while moving the animals forward at a constant velocity. The animals were tested without and with a chemical neuromodulation consisting of a serotoninergic replacement therapy that enables locomotion after spinal cord injury. Stick diagram decomposition of hindlimb movements is shown together with the electromyographic activity of flexor and extensor muscles. The shaded areas correspond to the stance phase of gait. The green dotted line indicates the onset of the constant-speed robotic forward actuation over a distance of 70 cm.

this purpose, we designed an experiment to control the output of ankle extensor muscle during locomotion through the modulation of vertical robotic trunk assistance. First, we performed a system identification. Spinal cord contused rats received the serotoninergic replacement therapy and were tested under different levels of vertical trunk assistance while the robotic interface moved them in the forward direction (position-control mode, 13 cm s^{-1}). A PC analysis was applied on 111 parameters derived from hindlimb kinematics, ground reaction forces, and muscle activity signals. The PC1, which explained 18% of variance, distinguished the different levels of vertical assistance ($P < 0.001$; figure 10(a)). Analysis of the parameters loading on PC1 revealed a robust correlation between the mean amplitude of extensor muscle activity and the level of vertical assistance ($r = -0.94$; figure 10(a)). Second, we designed a closed-loop control policy that updated the level of vertical trunk assistance based on the step-by-step evaluation of the extensor muscle activity. We programmed a proportional-integral (PI) controller that adapted the vertical trunk assistance in order to target a desired level of muscle activity at each step (figure 10(b)). We detected the step cycles based on the displacement of the foot with respect to the hip. The position of the hip and foot markers were monitored by the Vicon system, and transmitted in real-time to the robotic interface. The Euclidian distance between the hip and the foot markers was calculated online. Foot strikes were detected when the first derivative of the distance between the hip and the foot markers crossed a user-defined threshold. The muscle activity of the left ankle extensor muscle was continuously recorded at 2 kHz, rectified, and filtered with a moving average over 14 samples. The surface integral of the muscle activity burst was calculated after the detection of the stance phase onset. The measured signal served as feedback value, indicating the current state of muscle activity. To obtain a robust baseline, the muscle activity was recorded over three consecutive runs of approximately ten steps under vertical assistance corresponding to 50% of the rats' bodyweight. Third, we tested the performance of the controller. We implemented three reference values corresponding to 60%, 80% and 100% of the calculated baseline muscle activity that we tested in ascending and descending order (60%, 80%, 100%, 80%, 60%). The mean of controlled muscle activity reached the reference value with a maximal error of 5%. The level of vertical trunk assistance (blue crossed line in figure 10(c)) was continuously adapted in order to reach the reference muscle activity from step to step. As expected higher amplitudes of muscle activity

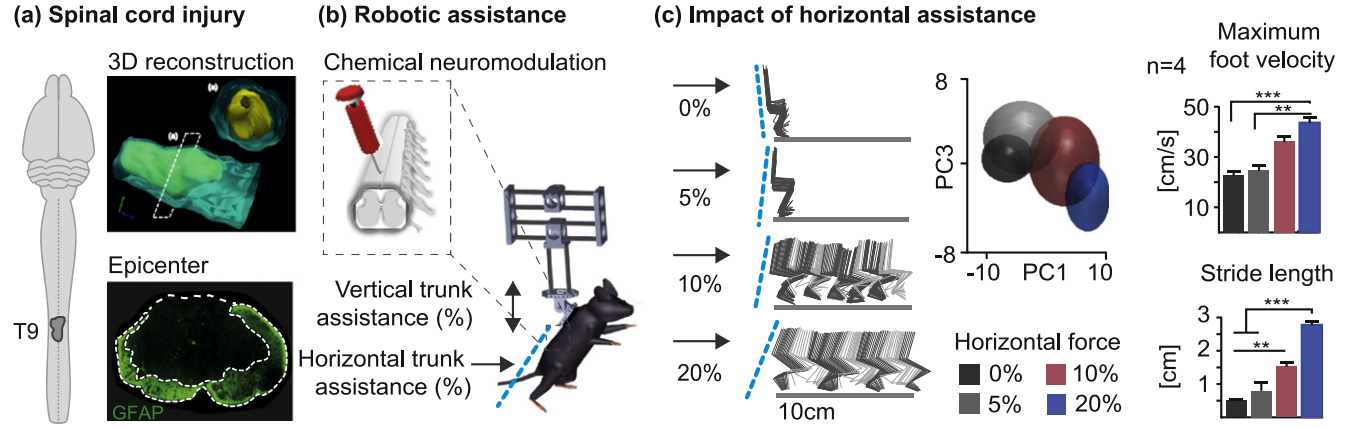

Figure 7. Impact of horizontal trunk assistance on gait execution in mice with spinal cord injury. (a) Four mice received a severe spinal cord contusion that spared less than 20% of tissue. 3D reconstruction of the lesion is shown together with the anatomical cross-section at the epicenter of the lesion. (b) Mice received a chemical neuromodulation therapy. They were tested with various degrees of horizontal trunk assistance and personalized vertical assistance. (c) Stick diagram decomposition of hindlimb movements with four levels of forward trunk assistance. Principal component (PC) analysis was applied on all a total of 98 variables quantifying various aspects of gait. Least-squares spheres were applied to individual gait cycles performed with a given horizontal trunk assistance to identify gait clusters. PC1, which accounted for 30% of the overall data variance, differentiated the different levels of forward trunk assistance. Bar graphs reporting average values of parameters that loaded on PC1, thus identifying the impact of forward trunk assistance on gait pattenrs ($n = 4$ mice). ** $P < 0.01$, *** $P < 0.001$. Error bars, s.e.m.

were associated with larger vertical ground reaction forces (figure 10(c)).

4. Discussion and conclusion

We have introduced a robotic interface that provides high-precision assistance of trunk movements along four independent degrees of freedom during both bipedal and quadrupedal locomotion in mice and rats. To hide the inertia of the massive robotic structure, we developed novel monolithic modules enabling selective compliance along specific degrees of freedom, which allowed high-fidelity force and torque control. The robotic interface instantly improved motor control in mice and rats with spinal cord injury. Moreover, we integrated this robotic interface within a real-time platform that supported closed-loop control of robotic actuations based on ongoing neural states. These results establish a technological framework for the development and mechanistic study of locomotor prosthetics and robot-assisted gait rehabilitation in rodent models.

4.1. High-precision assistance of multidirectional trunk movements

We aimed to develop a robotic interface capable of providing a dynamic, high-precision and gradual assistance of trunk movements in mice and rats while enabling unconstrained displacement in a large workspace. These features are conflicting. Indeed, fine control of forces over the small animal's trunk is not compatible with the displacement of a large-scale structure presenting substantial inertia and friction in the same degrees of freedom as the trunk attachment. We previously solved this complex robotic problem in rats using series elastic actuators expended in multiple directions (Dominici *et al* 2012). However, the bodyweight of mice is ten times smaller compared to rats, which prevented us from implementing the same concepts to build a robotic interface for these animals. To overcome this challenge, we exploited and combined the concepts of multidirectional series elastic actuation and selective compliance (Hasse and Campanile 2009) to render forces with high precision over a large workspace and in four independent degrees of freedom.

We tested the performance of the robot in advanced conditions including unconstrained locomotion of healthy, lightweight mice walking freely and at high speed along horizontal and vertical paths with changing directions. The dynamic conditions underlying these gait executions are incredibly demanding. Indeed, they expand well beyond the requirements that are expected for the development and evaluation of locomotor prosthetics in rodents with motor impairments. Yet, the robotic interface exhibited a high degree of performance during these tasks, minimally interfering with the gait patterns and balance of the mice. These results demonstrate that the performances of the robotic interface meet the requirements to evaluate, enable and train gait and balance in mouse and rat models of neuromotor disorders.

4.2. Integrated neurorobotic platform

We sought to establish an environment that enables the development of a broad range of prosthetic systems in both mice and rats. For this purpose, we selected, developed and integrated hardware and software that can be flexibly and rapidly combined to meet the needs of various experimental conditions or multiple modalities and types of prosthetics. For the robotic interface, we built rapidly interchangeable modules that are not only tailored to the animals' size, gait type and injury severity but also to the performed tasks. Along the

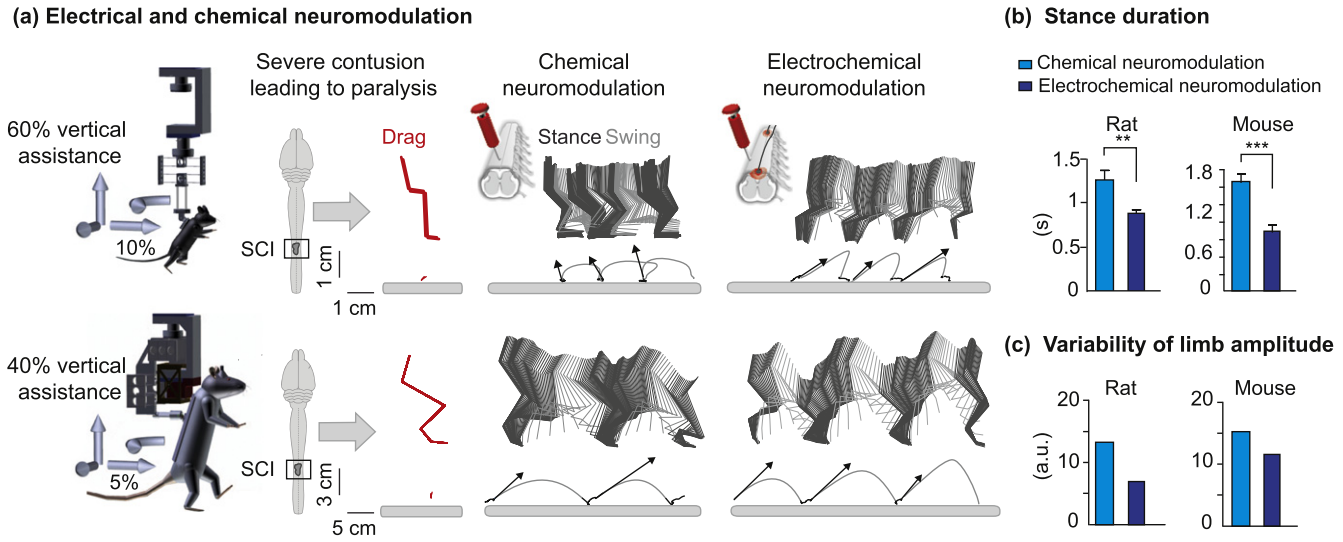

Figure 8. Synergistic facilitation of locomotion during electrical and chemical neuromodulation in mice and rats with spinal cord injury. (a) Mouse and rat with a spinal cord contusion leading to hindlimb paralysis were evaluated in the robotic interface without any neuromodulation, with chemical neuromodulation only, and with both electrical and chemical neuromodulation. The robotic interface provided personalized trunk assistance in the vertical and forward directions. Conventions are the same as in previous figures, except that foot trajectory and foot velocity (orientation and intensity of foot velocity vectors) at swing onset are also shown. (b), (c) Bar graphs reporting values of parameters that illustrate improved gait execution during electrical and chemical neuromodulation compared to chemical neuromodulation alone. Error bars, s.e.m. ** $P < 0.01$, *** $P < 0.001$.

same lines, the structure of the software enables switching from various control modes, or interfacing any recorded physiological signals with robotic or prosthetic actions. Therefore, we implemented the concept of modularity at both the software and hardware levels, creating a real-time environment wherein versatile experiments exploiting closed-loop control policies can be implemented effortlessly. To illustrate this versatility, we demonstrated the ability of the same robotic interface to enable coordinated weight-bearing locomotion in mice and rats with severe spinal cord injury, both quadrupedally and bipedally. This robotic environment allowed us to show the potential of electrical spinal cord stimulation to improve hindlimb motor control in mice, which had never been reported in this animal model. In combination with transgenic mouse models, this neurorobotic platform provides the opportunity to study the neurological mechanisms underlying the therapeutic effects of this paradigm. These experiments only required exchanging the selective compliant modules attached to a magnet. The trunk assistance mediated similar behavioral improvements in both rodent species. Second, we implemented a closed-loop control policy whereby the degree of vertical trunk assistance is continuously adjusted in order to target a desired amount of activity in anti-gravity muscles during locomotion in rats with spinal cord injury. This control policy may support the development of novel training paradigms wherein the degree of robotic assistance maximizes muscle activity, and thus, the overall amount of effort during rehabilitation. While the concept of modularity is often used in the design of single devices, we expanded this idea to multiple hardware and software configurations, enabling the realization of complex multi-system experiments within a short amount of time.

4.3. Development and evaluation of locomotor prosthetics in rodents

We configured the robotic interface to act as a postural or propulsive neuroprosthesis. To enable postural control, we adjusted the degree of multidirectional trunk assistance to the actual motor performance of the injured mice and rats. By reducing the impact of gravity on weight-bearing requirements and mediolateral balance, the robotic assistance instantly uncovered advanced locomotor capacities in mice with severe spinal cord injury. The complexity of gait execution without assistance dissimulated residual motor functions, which, however, were revealed under robotic assistance.

We also found that the degree of forward assistance was important to enable motor control in injured mice and rats. Previous studies have mainly focused on the impact of vertically-restricted trunk assistance, both in rodent models (Cai *et al* 2006, Udoekwere *et al* 2006, Hamlin *et al* 2015, Oza and Giszter 2014) and human patients (Finch *et al* 1991, van Hedel *et al* 2006, Labini *et al* 2011). Here, our results show that the robustness and quality of gait performance gradually improved with the addition of horizontal assistance. These preliminary findings emphasize the importance of expanding currently available trunk support systems, which are exclusively unidirectional, to multiple dimensions. To address this question, we recently co-developed a robotic trunk interface that is capable of providing human patients with adjustable multidirectional trunk assistance during unconstrained locomotion (Vallery *et al* 2013).

Our neurorobotic interface will play a pivotal role in the development of next-generation locomotor prosthetics and evidence-based algorithms for multidirectional trunk

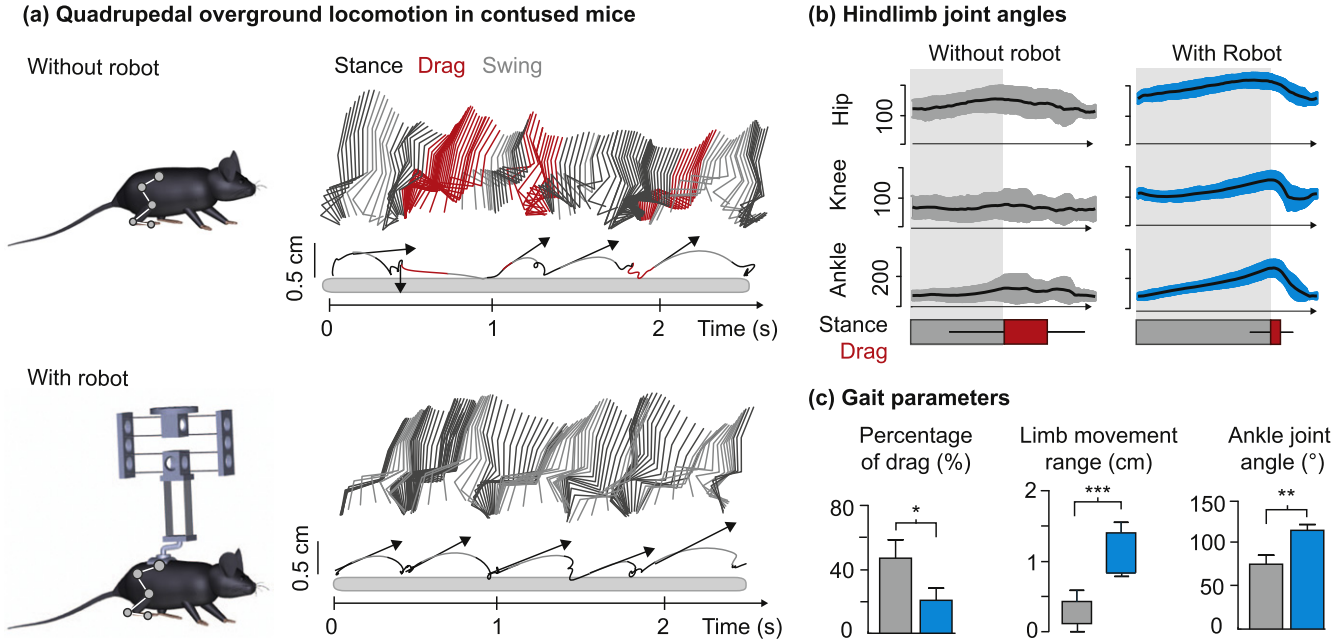

Figure 9. Robotic trunk assistance improves quadrupedal locomotion in mice with spinal cord injury. (a) A mouse that received a spinal cord contusion leading to hindlimb motor deficits was tested with and without personalized trunk assistance in the vertical direction. Conventions are the same as in figure 8. (b) Averaged changes in hindlimb joint oscillations (±s.e.m) are represented in both conditions. (c) Bar graphs reporting the average ($n = 10$ steps) values of relevant gait parameters in both conditions. $^{*}P < 0.05$, $^{**}P < 0.01$, $^{***}P < 0.001$.

assistance during rehabilitation. This framework will also support the study of the neurological mechanisms underlying the effects of prosthetic use and gait rehabilitation using advanced genetic tools in rats and mutant mouse models.

Acknowledgments

We would like to thank Isabel Vollenweider for her support with animal training and adjustment of the robot interface; Natalia Pavlova for performing the surgeries; and Pavel Musienko for his support in the elaboration of the attachment between the mice and the robotic support system. Financial support was provided by an individual grant (subside 310030_130850) and the National Center of Competence in Neural Repair and in Robotics of the Swiss National Science Foundation (51AU40_125773), the Bertarelli Foundation and a Starting Grant from the European Research Council [ERC 261247, Walk Again].

Appendix A

Under linear assumptions, the stiffness k_x of the soft DoF and maximum occurring stress $\sigma_{\max}$ within the beams of the simple parallel hinge can be calculated as follows (Smith 2000):

$$F_x = k_x u_x = \frac{2Ebt^3}{l^3} u_x, \tag{A.1}$$

$$\sigma_{\max} = \frac{3F_x l}{2bh^3}, \tag{A.2}$$

where b, t and l are the width, thickness and length of the plate, and E is the elasticity modulus of the corresponding material.

Essentially, the complex parallel hinge is a mirrored serial arrangement of two simple parallel hinges and therefore its stiffness and its maximum stress are given by

$$k_x = \frac{2Ebt^3}{l^3}, \tag{A.3}$$

$$\sigma_{\max} = \frac{3F_x l}{4bh^3}. \tag{A.4}$$

The rotational stiffness of the cross striped pivot is given by

$$k_\theta = n\frac{Ebt^3}{12l}, \tag{A.5}$$

where n is the number of beams. The maximum stress within the bending beams of this hinge is approximately given by:

$$\sigma_{\max} \approx \frac{Et}{2l}\theta_{\max}. \tag{A.6}$$

The geometric dimensions and the material for each hinge must be defined such that the stiffness and strength requirements are fulfilled. A suitable set of parameters for the used modules is given in table A1. It can be observed that the stiffness values meet the desired stiffness. The stress under applied motion remains below the maximum allowable stress.

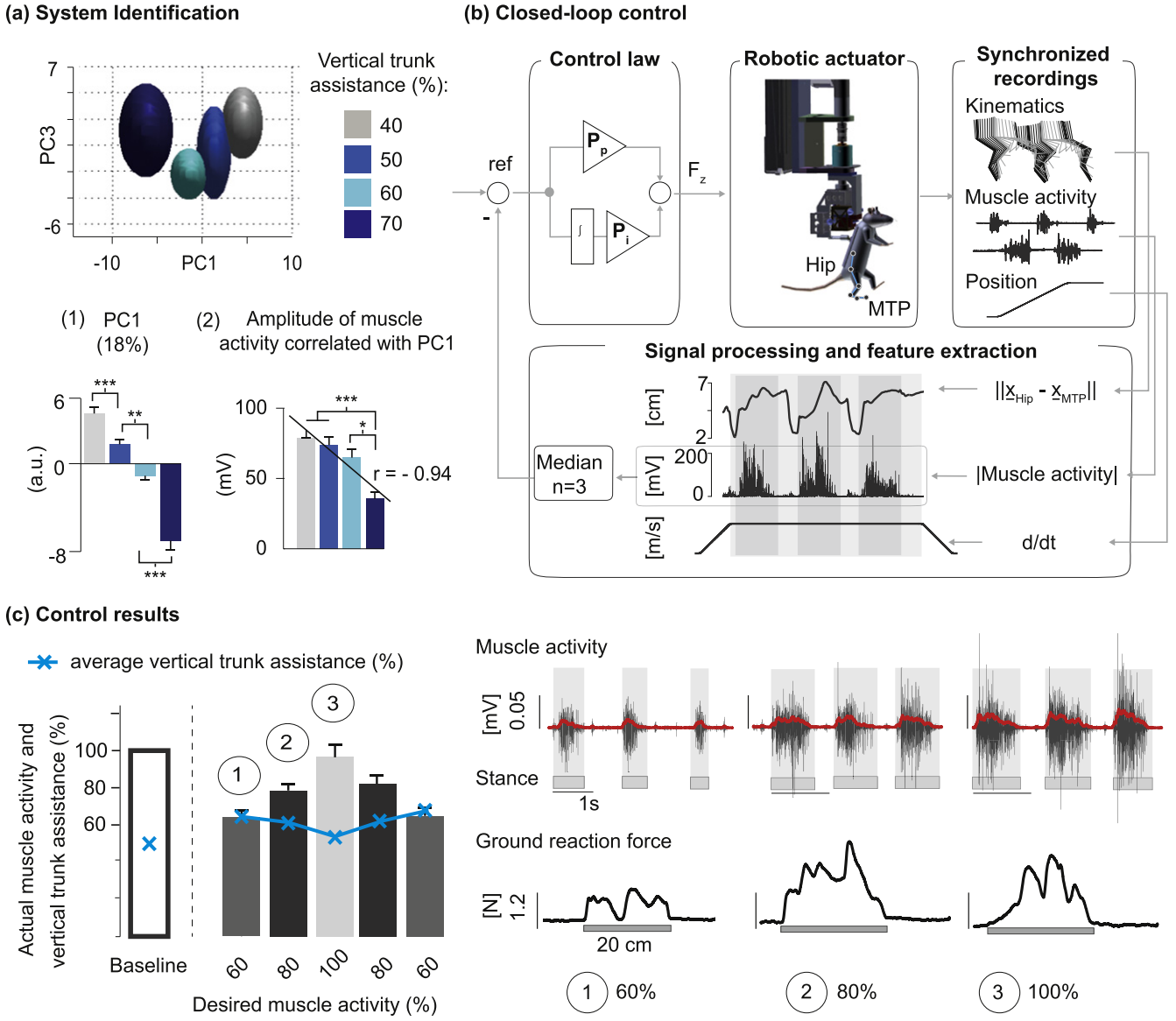

Figure 10. Closed-loop robotic control of muscle activity (a) Rat with a spinal cord contusion was tested during bipedal locomotion with vertical trunk assistance while the robot moved the rat forward at a constant velocity (13 cm s^{-1}). PC analysis was applied on a total of 111 variables quantifying gait patterns performed with various levels of vertical trunk assistance. Bar plots reporting mean values of scores on PC1 for the different levels of vertical trunk assistance, and the modulation of muscle activity recorded in ankle extensor muscles that significantly correlated with PC1 ($r = -0.93$). (b) We implemented a closed-loop proportional-integral (PI) controller that adjusted the level of vertical trunk assistance based on real-time recordings of muscle activity in the ankle extensor gastrocnemius medialis. Successive foot strikes were detected from kinematic measurements. (c) Bar graph reporting the measured muscle activity during baseline and while targeting different levels of muscle activity, as indicated along the *X*-axis. The blue crossed line indicate the level of vertical trunk assistance during each condition. Representative raw signals and rectified/filtered muscle activity are shown together with vertical ground reaction forces for three different levels of desired muscle activity.

Appendix B

To characterize force control performance, a force-tracking experiment was conducted following the procedure described previously (Parietti *et al* 2011): the end effector is manually restrained while the device is given a reference sinusoidal force that varies both in amplitude and frequency. Frequency slowly increases from 0.6 to 10 Hz, with multiple oscillations for each frequency, while amplitude decreases from 0.1 to 0.06 N. The force measured with the ATI force sensor is then compared to the reference force in terms of phase lag and amplification in steady state for each frequency. The experiment was conducted for the vertical axis with the 3D selective compliant module (module I in figure 1). The obtained bandwidth for this configuration is in the order of 3 Hz.

Table A1. Mechanical properties of compliant hinges.

	E (MPa)	b (mm)	t (mm)	l (mm)	$k_{x/\theta}$ (N m^{-1}) (Nmm/°)	k_{desired} (N m^{-1}) (Nmm/°)	$\sigma_{\max}$ (MPa)	σ_{allowed} (MPa)
Simple parallel hinge	210 000	10	0.05	30	19	20	180	500
Complex parallel hinge	210 000	10	0.05	23	43	40	138	500
Cross strip pivot	1500	5	0.5	14	0.19	0.20	7	30

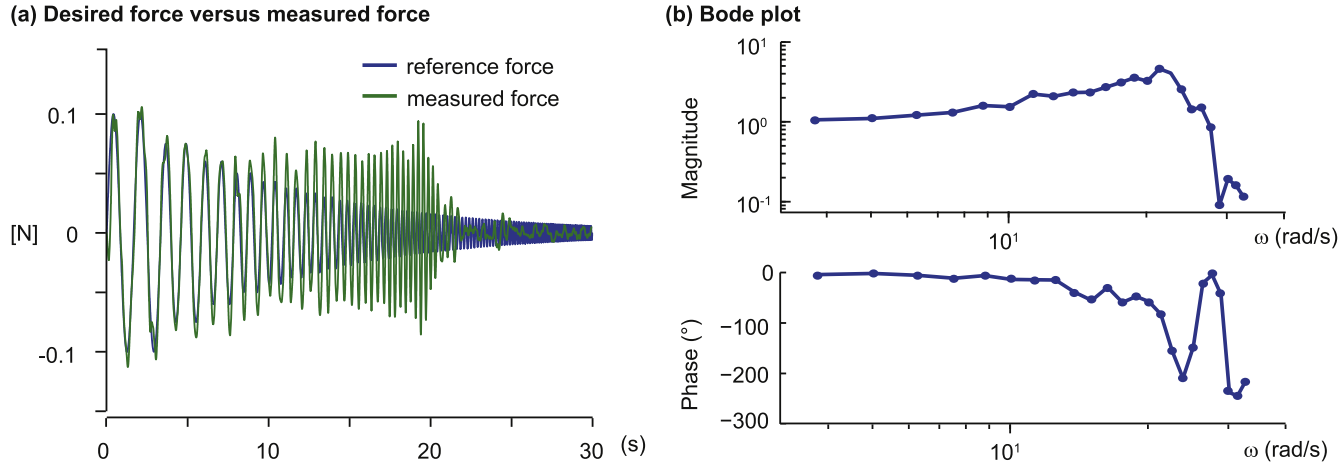

Figure B1. (a) Desired force versus force measured with the ATI force sensor installed above the selective compliant module. (b) Bode plot obtained from the force tracking experiment.

References

Angeli C A, Edgerton V R, Gerasimenko Y P and Harkema S J 2014 Altering spinal cord excitability enables voluntary movements after chronic complete paralysis in humans *Brain* **137** 1394–409

Barthelemy D, Leblond H and Rossignol S 2007 Characteristics and mechanisms of locomotion induced by intraspinal microstimulation and dorsal root stimulation in spinal cats *J. Neurophysiol.* **97** 1986–2000

Cai L L, Fong A J, Otoshi C K, Liang Y, Burdick J W, Roy R R and Edgerton V R 2006 Implications of assist-as-needed robotic step training after a complete spinal cord injury on intrinsic strategies of motor learning *J. Neurosci.* **26** 10564–8

Colgate E and Hogan N 1989 An analysis of contact instability in terms of passive physical equivalents *Proc. IEEE Int. Conf. on Robotics and Automation (ICRA) 1989* vol 1–3 pp 404–9

Courtine G and Bloch J 2015 Defining ecological strategies in neuroprosthetics *Neuron* **86** 29–33

Courtine G *et al* 2009 Transformation of nonfunctional spinal circuits into functional states after the loss of brain input *Nat. Neurosci.* **12** 1333–42

Dietz V and Harkema S J 2004 Locomotor activity in spinal cord-injured persons *J. Appl. Physiol.* **96** 1954–60

Dominici N, Keller U, Vallery H, Friedli L, van den Brand R, Starkey M L, Musienko P, Riener R and Courtine G 2012 Versatile robotic interface to evaluate, enable and train locomotion and balance after neuromotor disorders *Nat. Med.* **18** 1142–7

Duda G N *et al* 2014 Changing the mindset in life sciences toward translation: a consensus *Sci. Transl. Med.* **6** 264cm12

Edgerton V R *et al* 2008 Training locomotor networks *Brain Res. Rev.* **57** 241–54

Eppinger S D and Seering W P 1987 Understanding bandwidth limitations in robot force control *Proc. IEEE Int. Conf. on Robotics and Automation (ICRA)* pp 904–9

Finch L, Barbeau H and Arsenault B 1991 Influence of body weight support on normal human gait: development of a gait retraining strategy *Phys. Therapy* **71** 842–55

Fong A J, Cai L L, Otoshi C K, Reinkensmeyer D J, Burdick J W, Roy R R and Edgerton V R 2005 Spinal cord-transected mice learn to step in response to quipazine treatment and robotic training *J. Neurosci.* **25** 11738–47

Hamlin M, Traughber T Jr, Reinkensmeyer D J and de Leon R D 2015 A novel device for studying weight supported, quadrupedal overground locomotion in spinal cord injured rats *J. Neurosci. Methods* **246** 134–41

Hasse A and Campanile L F 2009 Design of compliant mechanisms with selective compliance *Smart Mater. Struct.* **18** 115016

Hsieh F and Giszter S 2011 Robot-driven spinal epidural stimulation compared with conventional stimulation in adult spinalized rats *Proc. IEEE Int. Conf. on Engineering in Medicine and Biology Society (EMBC)* (IEEE) pp 5807–10

Labini F S, Ivanenko Y P, Cappellini G, Gravano S and Lacquaniti F 2011 Smooth changes in the EMG patterns during gait transitions under body weight unloading *J. Neurophysiol.* **106** 1525–36

Mushahwar V K, Jacobs P L, Normann R A, Triolo R J and Kleitman N 2007 New functional electrical stimulation approaches to standing and walking *J. Neural. Eng.* **4** S181–97

Musienko P, van den Brand R, Marzendorfer O, Roy R R, Gerasimenko Y, Edgerton V R and Courtine G 2011 Controlling specific locomotor behaviors through multidimensional monoaminergic modulation of spinal circuitries *J. Neurosci.* **31** 9264–78

Nishimura Y, Perlmutter S I and Fetz E E 2013 Restoration of upper limb movement via artificial corticospinal and musculospinal

connections in a monkey with spinal cord injury *Front. Neural. Circuits* **7** 57

Oza C S and Giszter S F 2014 Plasticity and alterations of trunk motor cortex following spinal cord injury and non-stepping robot and treadmill training *Exp. Neurol.* **256** 57–69

Oza C S and Giszter S F 2015 Trunk robot rehabilitation training with active stepping reorganizes and enriches trunk motor cortex representations in spinal transected rats *J. Neurosci.* **35** 7174–89

Parietti F, Baud-Bovy G, Gatti E, Riener R, Guzzella L and Vallery H 2011 Series viscoelastic actuators can match human force perception *IEEE-ASME Trans. Mech.* **16** 853–60

Pratt G A and Williamson M M 1995 Series elastic actuators *Proc. IEEE/RSJ Int. Conf. on Intelligent Robots and Systems: (IROS) 1995* pp 399–406

Pratt G A, Williamson M M, Dillworth P, Pratt J, Ulland K and Wright A 1995 Stiffness isn't everything *Int. Symp. on Experimental Robotics (ISER)* pp 253–62

Reinkensmeyer D J, Aoyagi D, Emken J L, Galvez J A, Ichinose W, Kerdanyan G, Maneekobkunwong S, Minakata K, Nessler J A and Weber R 2006 Tools for understanding and optimizing robotic gait training *J. Rehab. Res. Dev.* **43** 657–70

Smith S T 2000 *Flexures: Elements of Elastic Mechanisms* (Boca Raton, FL: CRC Press)

Song W and Giszter S F 2011 Adaptation to a cortex-controlled robot attached at the pelvis and engaged during locomotion in rats *J. Neurosci.* **31** 3110–28

Song Y S and Hogan N 2008 Design of an overground interactive therapeutic robot for rodents recovering after spinal cord injury *Proc. ASME Dynamic Systems and Control Conf. 2008* pp 409–11

Song Y S, Sun Y, van den Brand R, von Zitzewitz J, Micera S, Courtine G and Paik J 2013 Soft robot for gait rehabilitation of spinalized rodents *2013 IEEE/RSJ Int. Conf. on Intelligent Robots and Systems (IROS)* pp 971–6

Steuer I, Rouleau P and Guertin P A 2013 Pharmacological approaches to chronic spinal cord injury *Curr. Pharm. Des.* **19** 4423–36

Takeoka A, Vollenweider I, Courtine G and Arber S 2014 Muscle spindle feedback directs locomotor recovery and circuit reorganization after spinal cord injury *Cell* **159** 1626–39

Timoszyk W K, Nessler J A, Acosta C, Roy R R, Edgerton V R, Reinkensmeyer D J and de Leon R 2005 Hindlimb loading determines stepping quantity and quality following spinal cord transection *Brain Res.* **1050** 180–9

Udoekwere U I, Oza C S and Giszter S F 2014 A pelvic implant orthosis in rodents, for spinal cord injury rehabilitation, and for brain machine interface research: construction, surgical implantation and validation *J. Neurosci. Methods* **222** 199–206

Udoekwere U I, Ramakrishnan A, Mbi L and Giszter S F 2006 Robot application of elastic fields to the pelvis of the spinal transected rat: a tool for detailed assessment and rehabilitation *Proc. Int. Conf. of the IEEE Engineering in Medicine and Biology Society (EMBC) 2006* pp 3684–7

Vallery H, Lutz P, von Zitzewitz J, Rauter G, Fritschi M, Everarts C, Ronsse R, Curt A and Bolliger M 2013 Multidirectional transparent support for overground gait training *Proc. IEEE Int. Conf. on Rehabilitation Robotics (ICORR)* pp 1–7

Vallery H, Veneman J, van Asseldonk E, Ekkelenkamp R, Buss M and van der Kooij H 2008 Compliant actuation of rehabilitation robots—benefits and limitations of series elastic actuators *IEEE Robot. Autom. Mag.* **15** 60–9

van den Brand R *et al* 2012 Restoring voluntary control of locomotion after paralyzing spinal cord injury *Science* **336** 1182–5

van Hedel H J, Tomatis L and Muller R 2006 Modulation of leg muscle activity and gait kinematics by walking speed and bodyweight unloading *Gait Posture* **24** 35–45

Waeber A, Gerig N, Baur K, Vallery H, Lutz P, Riener R, Curt A, Bolliger M and Rauter G 2015 Guidance in the nullspace reduces task difficulty in robot-assisted coordination training *Proc. IEEE Int. Conf. on Rehabilitation Robotics (ICORR)* pp 642–7

Wenger N, Moraud E M, Raspopovic S, Bonizzato M, Digiovanna J, Musienko P, Morari M, Micera S and Courtine G 2014 Closed-loop neuromodulation of spinal sensorimotor circuits controls refined locomotion after complete spinal cord injury *Sci. Transl. Med.* **6** 255ra133

Winter D A, Mackinnon C D, Ruder G K and Wieman C 1993 An integrated EMG/biomechanical model of upper body balance and posture during human gait *Prog. Brain Res.* **97** 359–67